Computational Model of Bone Remodeling Integrating Osteocyte Mechanotransduction and Microdamage-Driven Self-Repair

Diego A. Garzón-Alvarado[1,2,*], Carlos A. Duque-Daza[2], Juan Jairo Vaca-González[3], Estevam Barbosa Las Casas[4], Dorian L. Linero[5], Gregory de Boer[6], Raj Das[7], and Salah Ramtani[8]

[1]*Biotechnology Institute, Universidad Nacional de Colombia, Colombia*
[2]*GNUM, Universidad Nacional de Colombia, Colombia*
[3]*Escuela de Pregrado - Direccion Académica, Universidad Nacional de Colombia*
[4]*Universidade Federal de Minas Gerais (UFMG), Belo Horizonte, Brazil*
[5]*Civil and Agricultural Department, Universidad Nacional de Colombia, Colombia*
[6]*School of Mechanical Engineering, University of Leeds, United Kingdom*
[7]*School of Engineering, RMIT University, Australia*
[8]*Laboratoire CSPBAT, equipe LBPS, CNRS (UMR 7244),Universit e Sorbonne Paris Nord, France*
[*]*Corresponding author: Diego A. Garzón-Alvarado, dagarzona@unal.edu.co*

Abstract

Bone remodeling is a fundamental physiological process that maintains skeletal integrity through a tightly regulated balance between bone resorption and formation. Mathematical modeling provides a powerful framework for understanding the complex regulatory mechanisms underlying this process, particularly the interplay between biomechanical stimuli and cellular dynamics. This study introduces a new mathematical model of bone remodeling designed to capture the temporal evolution of key bone cell populations and their response to mechanical stimuli within a simplified yet biologically informed architecture. We formulate a system of coupled nonlinear ordinary differential equations to describe the dynamics of osteoclasts, osteoblasts, and osteocytes within a single basic multicellular unit (BMU). The model incorporates feedback regulation via strain energy density, allowing mechanical input to influence cellular activity and bone surface transitions. Initial conditions are assigned to reflect the sequential activation of bone remodeling phases. Physiological parameters are adopted from well-established literature, while non-sourced parameters are tuned to ensure model stability and biological plausibility. The simulations reproduce the canonical sequence of bone remodeling: initiation, resorption, reversal, and formation. The model captures the coupling between mechanical loading and cellular activity, demonstrating how osteocyte signaling can modulate the recruitment of osteoclasts and osteoblasts. The results also highlight the system's capacity to stabilize around a dynamic equilibrium, sensitive to both internal parameters and external mechanical inputs. This model offers a minimal yet comprehensive representation of bone remodeling dynamics within a single BMU, integrating mechanical and biological controls into a unified mathematical structure. It provides a foundation for future extensions toward spatially distributed models and applications in mechanobiological simulation and computational bone health assessment.

Keywords— Bone remodeling, Komarova's model, osteoclasts, osteoblasts, osteocytes

1 Introduction

Human bone remodeling is an intricate process governed by the complex interplay of biology and mechanics. This process, mediated by osteoblasts and osteoclasts within the basic multicellular unit (BMU), has been studied for centuries, providing a deeper understanding of the relationship between bone geometry and the mechanical forces influencing it. The groundbreaking works of German surgeon Julius Wolff, German civil engineer Karl Culmann, and Swiss anatomist Georg Hermann Von Meyer, along with the American orthopedic surgeon Harold Frost, have significantly shaped our comprehension of the underlying mechanisms of bone remodeling.

Julius Wolff, in the latter part of the 19th century, laid the foundation of what is now recognized as Wolff's Law of Bone Transformation [7, 58]. Through meticulous observations in dissection rooms and the study of museum

specimens, Wolff postulated three fundamental principles concerning the internal architecture of the bone and its trabecular arrangement [56, 57].

Firstly, the internal architecture of bone, primarily composed of trabeculae, exhibits a consistent pattern within a specific bone across different individuals. Secondly, most trabecular lines intersect at right angles, and thirdly, deformation or fracture can alter the arrangement of trabeculae, but over time, they will reorient to conform to the second principle [58]. His insightful observations introduced the concept of bone remodeling and adaptation, highlighting the dynamic nature of bone as a living tissue.

As discussed by [9], Wolf drew inspiration from Culmann and Von Meyer, who had further envisaged the relationship between mechanical loads and the geometry of bone structure, with a specific emphasis on the alignment of trabeculae [15, 47, 51]. Culmann was particularly interested in understanding how mechanical forces affect bone structure, striving to illustrate this relationship mathematically [16]. Simultaneously, Von Meyer highlighted the regular internal system found in most human bones, revealing the intricate design that bones possess [52].

Fast-forwarding to the 20th century, Harold Frost made substantial contributions to our understanding of skeletal deformities during development, using mammalian skeletons as his primary subjects of study [19]. Frost proposed that bone structure requires continuous modeling and remodeling to adapt to mechanical loads, a concept that echoed Wolff's initial postulates and provided a significant advancement to the field of bone biology. He also noted that bone resorption can occur near the bone marrow, hinting towards the role of the bone microenvironment in influencing bone remodeling [20]. Frost introduced the term "mechanostat" to describe the mechanism responsible for monitoring bone metabolism, specifically within the BMU, signifying the coupling and activation of osteoblasts and osteoclasts [21].

A new generation of multiscale models that integrate mechanical stimuli with biochemical and structural regulators. Pivonka et al. [41] developed a multiscale model capturing geometrical regulation through dynamic bone surface availability. This approach offers key insights into disease progression, particularly osteoporosis, by linking porosity and stiffness to cellular behavior. Similarly, Pastrama et al. [39] incorporated pore-specific mechanosensation into a poromicromechanical model, simulating how load frequency and pore morphology modulate bone adaptation.

Alternative formulations emphasize systemic dynamics. Zumsande et al. [62] applied generalized modeling and bifurcation analysis to explore global properties of remodeling systems, identifying thresholds that could precipitate pathologies like Paget's disease. In another direction, Chen-Charpentier and Diakite [11] incorporated delays in osteocytic signaling and differentiation, revealing oscillatory remodeling behavior and enhancing the biological realism of time-dependent remodeling phenomena.

Another axis of development concerns remodeling in response to implants and aging. Mathai et al. [33] proposed a topology-optimized remodeling algorithm for uncemented femoral implants, surpassing isotropic and orthotropic models in predictive accuracy, especially in structurally sensitive regions like Ward's triangle.

In addition, Huo et al. [26] introduced physiological stochasticity into topology optimization, achieving realistic morphologies in elderly and adult bones, thus improving relevance to patient-specific scaffold design. Pawlikowski et al. [40] highlighted a mechanobiological driver—angiogenesis—in osteoarthritis modeling. Their review identified critical scaling issues and called for integration of personalized mechanical and biochemical inputs. Along similar translational lines, Wan et al. [53] linked bone remodeling with fatigue in mandibular plates using XFEM, providing a dynamic tool for implant optimization. While these works expand clinical translation, the mechanical-structural feedback in long-term adaptive remodeling of implants is underexplored, especially in vivo.

Electromechanical and pharmacological feedback mechanisms are also gaining traction. Fernández et al. [18] explored piezoelectric signaling in bone, proposing that curvature-induced electric fields guide osteoblastic/osteoclastic activity, effectively merging structural and electrical cues. Bahia et al. [2] offered a PBPK-driven model integrating drug diffusion and bone cell dynamics. Their framework simulates therapeutic interventions under osteoporotic conditions, opening doors to personalized medicine.

Alternatively, other computational models have been developed to capture the biological and mechanical complexities of bone remodeling. One of the earliest and most influential contributions was made by Weinans et al. [54], who proposed a strain energy-based remodeling rule implemented within a finite element framework [54]. Their model introduced the concept of bone as a self-optimizing material, adapting its density locally to achieve a target mechanical stimulus. This approach produced density distributions that closely resembled physiological trabecular patterns and laid the groundwork for subsequent finite element-based simulations. Building upon this mechanistic foundation, Komarova et al. [29] introduced a biologically-driven model that incorporates the dynamic interactions between osteoblasts and osteoclasts [29]. Using a system of nonlinear differential equations, their framework captures both autocrine and paracrine regulation of bone cell populations. This model reproduces key physiological behaviors such as single-cycle and continuous remodeling, and it offers insights into pathological states like Paget's disease through its prediction of unstable oscillatory dynamics.

Further developments in the numerical implementation of remodeling models have been explored by Garzón-Alvarado and Linero [23], who evaluated the influence of different time integration schemes—Euler, Heun, and Runge–Kutta—on the evolution of bone density in computational simulations. Their work demonstrated that while all schemes can qualitatively replicate remodeling patterns, the numerical precision and stability can significantly vary depending on the integration method and discretization strategy [23].

In the domain of theoretical and stochastic modeling, Lemaire et al. [31] presented a landmark cellular model incorporating RANK/RANKL/OPG signaling. Their model successfully simulates hormonal therapies and various metabolic bone disorders. Liò et al. [32] contributed a unique stochastic and algebraic approach using Shape Calculus to bridge cellular and tissue-level interactions, capturing the discrete stochastic behavior of BMUs. Baiotto et al. [3] simulated unloading-induced remodeling under microgravity using rat tail-suspension data, reinforcing the role of osteocyte distribution in mechanotransduction. Additionally, Papathanasopoulou et al. [38] proposed a poroelastic formulation using Biot's consolidation theory to study internal remodeling influenced by medullary implants. Zidi and Ramtani [61] offered a nonlinear dynamical systems perspective, using finite-difference schemes to study global stability in trabecular adaptation, demonstrating how local feedback can lead to global architectural changes. Moroz and Wimpenny [35] introduced a cybernetic model based on allosteric regulation within BMUs. Their use of classical enzymatic regulation paradigms (e.g., Hill, MWC) reveals possible cyclic attractors and offers scaffold design principles grounded in robust biological control theory.

In addition, osteoblastogenesis is equally regulated by a complex interplay of transcription factors and cytokine networks. The canonical Wnt/β-catenin signaling pathway is vital for osteoblast differentiation from mesenchymal stem cells. Binding of Wnt ligands to Frizzled and LRP5/6 co-receptors inhibits β-catenin degradation, allowing its accumulation and nuclear translocation where it promotes transcription of osteogenic genes. This pathway is tightly regulated by antagonists like sclerostin and DKK1, predominantly secreted by osteocytes. Mechanical loading reduces expression of these inhibitors, thereby enhancing Wnt signaling and bone formation [28]. Bone morphogenetic proteins (BMPs), particularly BMP2 and BMP7, further stimulate osteoblast differentiation through the Smad1/5/8 pathway, promoting the expression of key transcription factors including Runx2 and osterix. Runx2 acts as a master regulator of osteogenesis, necessary for the commitment of progenitor cells to the osteoblast lineage, while osterix is indispensable for the maturation of preosteoblasts.

Osteoblast differentiation is modulated by a wide array of cytokines. Pro-osteogenic cytokines such as IL-10, IL-11, IL-18, and IFN-γ enhance osteoblast differentiation, whereas cytokines like TNF-α, IL-1β, and IL-7 exert anti-osteogenic effects. These cytokines influence the expression of Runx2, ATF4, and AP-1, which coordinate the transcriptional machinery governing osteoblast function. Notably, SATB2, a chromatin remodeler, synergizes with Runx2 and ATF4 to promote the expression of osteogenic markers such as osteocalcin and bone sialoprotein. The integration of these signals ensures a tightly regulated osteoblastogenesis that can respond to both systemic and local environmental cues [1].

Mechanical signals also play a critical role in regulating the bone remodeling process. Osteocytes, embedded within the mineralized matrix, act as mechanosensors that detect strain and orchestrate adaptive remodeling. Upon mechanical stimulation, osteocytes reduce the secretion of sclerostin and DKK1, thus unleashing Wnt/β-catenin signaling and promoting anabolic bone formation. In contrast, microdamage-induced osteocyte apoptosis triggers the recruitment of osteoclast and osteoblast precursors via paracrine signals, highlighting their dual role in initiating both resorption and formation phases of the remodeling cycle [28]. The bone remodeling cycle is not only a response to mechanical and metabolic demands but is also tightly coupled to systemic hormonal regulation. Parathyroid hormone (PTH) stimulates both osteoblast activity and RANKL expression, thereby influencing both arms of remodeling. Additionally, glucocorticoids, sex steroids, vitamin D, and thyroid hormones have profound effects on the signaling milieu that governs bone turnover.

Despite these strides, a key gap remains: few models simultaneously and comprehensively address the feedback loops between cellular differentiation, mechanosensation, and time-dependent regulation across scales. Future research must better integrate spatial and temporal resolution within physiologically validated frameworks.

This study presents a new conceptual framework for bone remodeling, emphasizing the intricate interplay between mechanical and biological elements. Our model represents a leap forward in comprehensively capturing and explaining the dynamic evolution of this physiological process. This model introduces a depiction of the self-repairing mechanism—an intrinsic goal of bone remodeling. This novelty from previous models underscores the commitment to representing the biological intricacies inherent in the remodeling process, providing a more holistic point of view.

Our model's unique strength lies in its simultaneous consideration of biological events, incorporating the Basic Multicellular Unit (BMU) of osteoclasts and osteoblasts, while also encompassing bone cells outside the BMU, such as osteocytes. This integration merges self-repairing biological processes with the mechanical dynamics of microdamage, resulting in a more realistic and unified representation. The communication channels among osteocytes, osteoblasts, and osteoclasts were utilized to describe the mechanisms governing bone remodeling. This model advances the bone remodeling approach by incorporating previously unexplored events like the self-repairing process and providing a comprehensive framework for deeper insights and potential applications in other pathological and physiological contexts, as demonstrated in the second part of this research.

It is important to remark, Bone remodeling is a dynamic and precisely orchestrated biological process essential for maintaining skeletal integrity, mineral homeostasis, and adapting to mechanical demands. It is mediated by a balance between osteoclast-mediated bone resorption and osteoblast-driven bone formation within the basic multicellular unit (BMU). Central to the regulation of this cycle are multiple signaling pathways that govern the differentiation, activation, and apoptosis of bone cells. Among these, the receptor activator of nuclear factor kappa-B ligand (RANKL), its receptor RANK, and the decoy receptor osteoprotegerin (OPG) constitute a pivotal signaling axis that controls osteoclastogenesis. RANKL is expressed by osteoblasts and osteocytes and binds to RANK on

osteoclast precursors, initiating a cascade involving NF-κB, c-Fos, and NFATc1, which are necessary for osteoclast differentiation and function. OPG, secreted by osteoblasts, competitively binds RANKL, preventing its interaction with RANK and thus inhibiting osteoclast formation and activity. The RANK/RANKL/OPG system is crucial not only in physiological bone turnover but also in pathological conditions such as osteoporosis and rheumatoid arthritis, where its dysregulation results in excessive bone resorption [6].

The primary objective of this work is to develop and validate a computational model of bone remodeling that integrates both mechanical and biological regulatory mechanisms, with a particular emphasis on the active role of osteocytes as mechanosensors and signaling mediators. Motivated by limitations in existing models—many of which omit osteocytes or treat them as passive participants—we build upon the foundational framework of Komarova et al. by incorporating osteocyte dynamics and mechanotransduction into the remodeling process.

Specifically, the proposed model captures how osteocytes detect mechanical stimuli, such as local strain energy density, and transduce these signals to modulate the behavior of osteoclasts and osteoblasts. This bidirectional feedback mechanism enables the simulation of adaptive remodeling in response to both mechanical loading and the accumulation of internal microdamage. A key innovation is the inclusion of a self-repair loop that dynamically resolves damage through osteoclast-mediated resorption and osteoblast-mediated formation, eliminating the need for artificial remodeling triggers. The model architecture couples a system of nonlinear ordinary differential equations representing the temporal dynamics of cellular populations and bone mass with a spatially-resolved continuum mechanics formulation solved using the Finite Element Method (FEM). This enables the simulation of spatially heterogeneous remodeling responses under physiologically relevant loading conditions. Damage evolution is computed from mechanical stress histories and regulated by a mass-slope-based sensor, which determines the activation of localized repair mechanisms.

One of the distinguishing features of the model is the asynchronous activation of Basic Multicellular Units (BMUs) across finite elements, which more accurately reflects the stochastic and spatially distributed nature of in vivo remodeling. As a result, the model reproduces emergent structural patterns consistent with known physiological phenomena, including the formation of anisotropic, load-bearing trabecular architectures. The novel contributions of this study include: (1) the explicit modeling of osteocytes as active regulators within a mechanobiological feedback loop; (2) the implementation of a dynamic, microdamage-driven self-repair mechanism; (3) the coupling of local mechanical states to global tissue-level remodeling outcomes; (4) results of the model here developed; and (5) the conclusions of this work. These advancements provide a biologically grounded and mechanically responsive framework capable of simulating both bone maintenance and repair in a physiologically plausible manner. This work serves as the foundation for further extensions, including the modeling of pathological remodeling scenarios such as metastatic bone disease or metabolic bone disorders.

The paper is organized as follows: a general description of the model is presented in the next section, where we provide many of the most essential details underlying the proposed framework. Next, we offer some validation with computational experiments using a very well known benchmark example.

2 Bone remodelling process: accounting for biological and mechanical inputs

The bone remodeling model introduced in this work considers the essential cellular components involved in bone formation, resorption, and maintenance, specifically osteoblasts, osteoclasts, and osteocytes. This model encapsulates the dynamic interplay between these cells, integrating accumulated damage and the effects of paracrine and autocrine factors. Figure 1 illustrates the model's general framework, delineating the information flow among cells and its implications for bone remodeling.

In this framework, osteocytes act as mechanosensors, detecting mechanical stimuli and coordinating the activities of osteoblasts and osteoclasts to facilitate a dynamic exchange of bone mass and effective removal of microdamage. A complex interaction between biological and mechanical factors regulates the remodeling process. Mechanically, it includes damage-induced stresses and loading, while biological aspects cover phenomena such as disease conditions, hormonal influences, and therapeutic interventions.

Osteocytes play a pivotal role within the bone cell community, orchestrating a comprehensive communication network that guides the remodeling process. This leads to an updated bone mass distribution and damage removal, thereby preserving or altering the tissue's mechanical properties. The stimulus of mechanical stress, depicted as orange lines in Figure 1, affects the osteocytes, serving as the control center for remodeling. Osteoclasts and osteoblasts, illustrated in blue, collaborate to eradicate damaged areas, with damage potentially exerting a reciprocal effect on both cells and surrounding tissue, possibly leading to organ collapse. The solid lines in Figure 1 represent communication between bone cells, ensuring synchronized efforts in maintaining tissue integrity and adapting to changes. The dashed black line indicates the influence of biological and metabolic events on the cells, underscoring the systemic impact on the bone remodeling process.

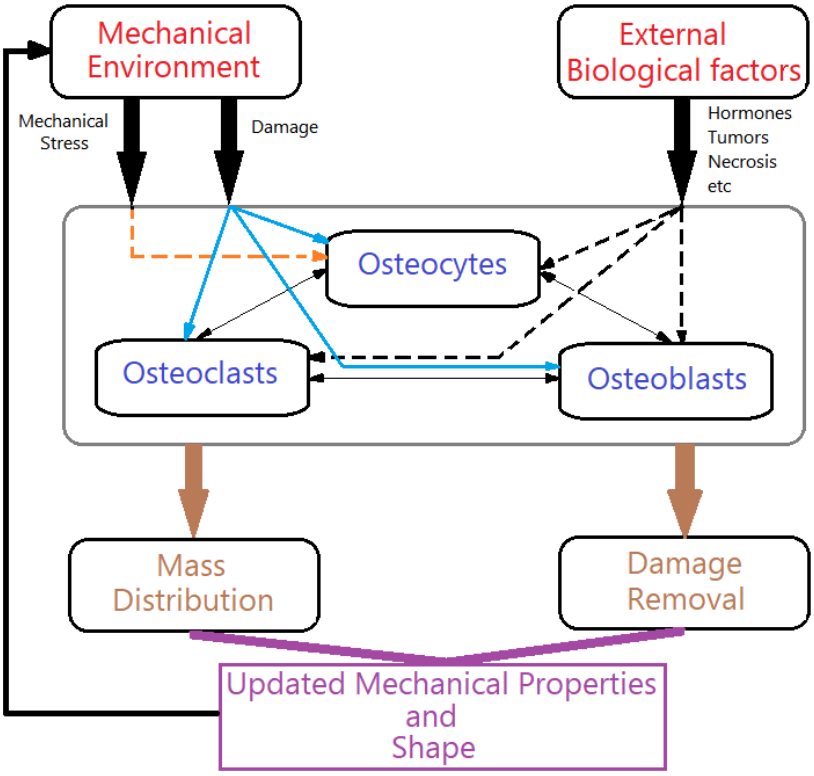

Figure 1: Biological and mechanical factors stimulate the bone remodeling process.

2.1 Mechanical Environment

Our model adopts a macroscopic approach, considering bone tissue as a continuous medium. However, the individual cells are explicitly accounted for within each element, and their influence on the tissue is evaluated through the incorporation of damage signals and cell coupling. According to the findings and results presented by Beaupré et al. [4], Carter [8], Cowin and Hegedus [13], Huiskes et al. [25], who have discussed the intricacies of the mechanical behavior of bone tissue, our model adopts a linear and homogeneous approach.

For the purpose of describing the effect of the mechanical environment, and without loss of generality, let us initially consider a two-dimensional domain, as depicted in Figure 2. In this general situation the domain Ω represents a continuum medium which is subjected to mechanical loads, also shown in Figure 2. While a 2D domain is employed for visual simplicity, it is crucial to emphasize that our model is universally applicable to arbitrary 3D domains where $\Omega \in \mathbb{R}^n$, with $n = 1, 2, 3$.

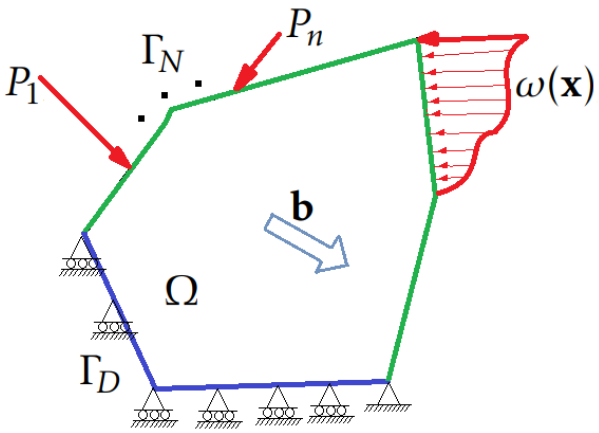

Figure 2: A general $2D$ domain Ω used to formulate the coupled model. $\omega(\mathbf{x})$: distributed mechanical load; $\mathbf{P_1}, ..., \mathbf{P_n}$: concentred mechanical loads; $\mathbf{b}$: body force; Γ: boundary set; Γ_N: Neumann Boundary (in green); Γ_D: Dirichlet boundary (in blue).

The applied loads can be distributed ($\omega(\mathbf{x})$) or concentrated at specific points ($\mathbf{P_1}, ..., \mathbf{P_n}$), thereby establishing the Neumann boundary conditions on Γ_N. Additionally, the mechanical system requires Dirichlet boundary conditions, which prescribe the displacement constraints of the body on Γ_D. Consequently, the boundary of the domain can be expressed as $\Gamma = \Gamma_N \bigcup \Gamma_D$, with $\Gamma_N \bigcap \Gamma_D = \emptyset$. The static form of the force balance equation, also known as the momentum equation and elaborated upon by Wriggers [59], can then be expressed as:

$$\nabla \cdot \sigma(\mathbf{x}, t) + \mathbf{b} = \mathbf{0}, \quad \forall \mathbf{x} \in \Omega, \tag{1}$$

$$\sigma(\mathbf{x}, t) \cdot \mathbf{n}(\mathbf{x}) = \omega(x), \quad \forall \mathbf{x} \in \Gamma_N, \tag{2}$$

$$\mathbf{u}(\mathbf{x}) = \mathbf{u_0}(\mathbf{x}), \quad \forall \mathbf{x} \in \Gamma_D \tag{3}$$

where $\sigma(\mathbf{x}, t)$ is the Cauchy Stress tensor at time t, $\mathbf{n}(\mathbf{x})$ is the outward-oriented unit vector, and $\mathbf{u_0}(\mathbf{x})$ is the field of fixed displacement. The stress-strain constitutive relation for the bone tissue is given by [23]:

$$\sigma(\mathbf{x}, t) = \mathbb{C}(\mathbf{x}, \mathbf{s}_{BMU}, \hat{D}(\mathbf{x}, t, \hat{\beta}_1)) : \varepsilon(\mathbf{x}, t), \tag{4}$$

where ε is the strain tensor given by $\varepsilon = \frac{1}{2}(\nabla \mathbf{u}(\mathbf{x}, t) + \nabla \mathbf{u}(\mathbf{x}, t)^T)$, and $\mathbb{C}(\mathbf{x}, \mathbf{s}_{BMU}, \hat{D}(\mathbf{x}, t, \hat{\beta}_1))$ is the elasticity tensor given by

$$\mathbb{C}(\mathbf{x}, \mathbf{s}_{BMU}, \hat{D}(\mathbf{x}, t, \hat{\beta}_1)) = (\alpha_m \cdot (s_0(\mathbf{x}, t))^{g_{0m}} \cdot (z(\mathbf{x}, t))^{g_{zm}}) \cdot \mathbb{C}_0, \tag{5}$$

where $s_0(\mathbf{x}, t)$ and $z(\mathbf{x}, t)$ are osteocytes and bone mass concentration at a material point $\mathbf{x}$ and at time t, respectively; g_{0m} and g_{zm} are constants that take into account the effect of osteocytes and bone mass on the elasticity tensor $\mathbb{C}$. In particular, in Equation (5) α_m is a function that takes into account the damage effect, given by

$$\alpha_m = 1 - \hat{D}(\mathbf{x}, t, \hat{\beta}_1), \tag{6}$$

Osteocytes communicate with osteoclasts ($s_1(\mathbf{x}, t)$) and osteoblasts ($s_2(\mathbf{x}, t)$) to control the deposition and resorption of bone tissue at a material point $\mathbf{x}$. The bone matrix, represented as a percentage $z(\mathbf{x}, t)$, is deposited and renewed by these cells. Collectively, the variables osteocytes, osteoclasts, osteoblasts, and bone mass percentage are combined into a state vector $\mathbf{s}_{BMU} = [s_0, s_1, s_2, z]^T$. It is pertinent to underscore that the inclusion of osteocytes within the set of Basic Multicellular Units (BMUs) is solely for representational purposes. In essence, osteocytes are not intrinsic members of the BMU; rather, the BMU primarily encompasses osteoclasts and osteoblasts, with osteocytes residing outside this delineation.. The term $g_{i\,m}$ describes the net effect of osteocytes (with $i = 0$) and bone mass percentage (with $i = z$) on the elasticity tensor of the mechanical properties. The mechanical damage, $\hat{D}(\mathbf{x}, t, \hat{\beta}_1)$, can be induced by external factors, such as highly concentrated stress leading to fractures or accumulated stresses over time. Furthermore, $\mathbb{C}_0$ represents the isotropic linear tensor with constants defining the linear material behavior, including the Young's modulus E and Poisson's ratio ν. In equation 5, one can observe the independent influence of mineralization and bone mass increase, attributed to osteocyte signaling in the bone remodeling process. This signaling ensures the ongoing maintenance of bone integrity. Furthermore, osteocytes also direct osteoblasts to enhance bone mass deposition through mineralization in response to mechanical loads, as emphasized by O'Brien et al. [37].

Following Datta et al. [17], the damage is accumulated over time due to microdamage in the tissue under mechanical stresses, given by

$$D(\mathbf{x}, t) = \sum_{\Delta t} \theta \sigma(\mathbf{x}, t) \Delta t \tag{7}$$

where θ is a constant representing the level of damage caused by the stress $\sigma(\mathbf{x}, t)$ over a specific time range Δt. The damage continuously accumulates in the tissue until it is resolved during remodeling. Osteoclasts are responsible for resorbing the damaged tissue, while osteoblasts generate new tissue at the site of microdamage. As a result, the damage is reset to zero at the beginning of each bone remodeling cycle. Therefore, there exists a sensor effector that detects changes in tissue density over time. In this study, the sensing is based on the bone mass percentage function, denoted as z, using a subset of temporal points of that z function ($-r-$ points) and incorporating a linear regression given by $\hat{z} = \hat{\beta}_0 + \hat{\beta}_1 t$, where $\hat{z}$ is the linear interpolation of z in r points. Consequently, the sensor considers the change in slope during the remodeling process, as illustrated in Figure 3. The expression for the sensor is as follows:

$$\hat{\beta}_1 = \frac{\sum_{i=1}^{r} (z_i t_i) - r \bar{z} \bar{t}}{\sum_{i=1}^{r} (z_i)^2 - \frac{1}{r} \left(\sum_{i=1}^{r} z_i \right)^2} \tag{8}$$

where t_i, and z_i are a couple of times and bone mass percentages for the i-th point in the interpolation; $\bar{z} = \frac{1}{r} \sum_{i=1}^{r} z_i$, $\bar{t} = \frac{1}{r} \sum_{i=1}^{r} t_i$ are the averages of the points for z and t, respectively. Figure 3 shows the $\hat{z}$ interpolation and the values of $\hat{\beta}_0$ and $\hat{\beta}_1$; this latter is the sensor of renewing of bone tissue; hence, the damage function is completed by

$$\hat{D}(\mathbf{x}, t, \hat{\beta}_1) = \begin{cases} 0 & \text{if } \hat{\beta}_1 < 0 \\ D(\mathbf{x}, t) & \text{if } \hat{\beta}_1 \geq 0 \end{cases} \tag{9}$$

By utilizing the damage equation 9, it becomes possible to identify instances where tissue replacement occurs and how microdamage accumulates over time. It is important to note that osteocytes perceive mechanical stress in terms of energy ($U = \frac{1}{2}\sigma : \varepsilon$) and communicate with osteoblasts and osteoclasts to enhance the mechanical properties of the bone as an organ. Additionally, damage can arise from an abnormal metabolic environment, as demonstrated in the subsequent sections that present the biological model for cells. Thus, in each material point, the progression of bone mass is computed over time to evaluate the extent of damage based on the biological and mechanical conditions within that specific point.

It is important to remark that fluid flow can be considered the primary mechanical signal sensed by osteocytes, triggering cellular responses and subsequent control signals over the Bone Multicellular Unit (BMU), including osteoclasts and osteoblasts [34, 50]. This perspective aligns with the findings of [45, 46], where computational evaluations comparing deformation energy and fluid flow demonstrate similar patterns of bone remodeling. However, [45, 46] underscore that while fluid flow can adequately induce remodeling signals and generate reasonable remodeling patterns, the Strain Energy Density signal accurately reflects physiological remodeling patterns. Therefore, this paper adopts Strain Energy Density as the primary mechanotransductive signal driving bone remodeling processes.

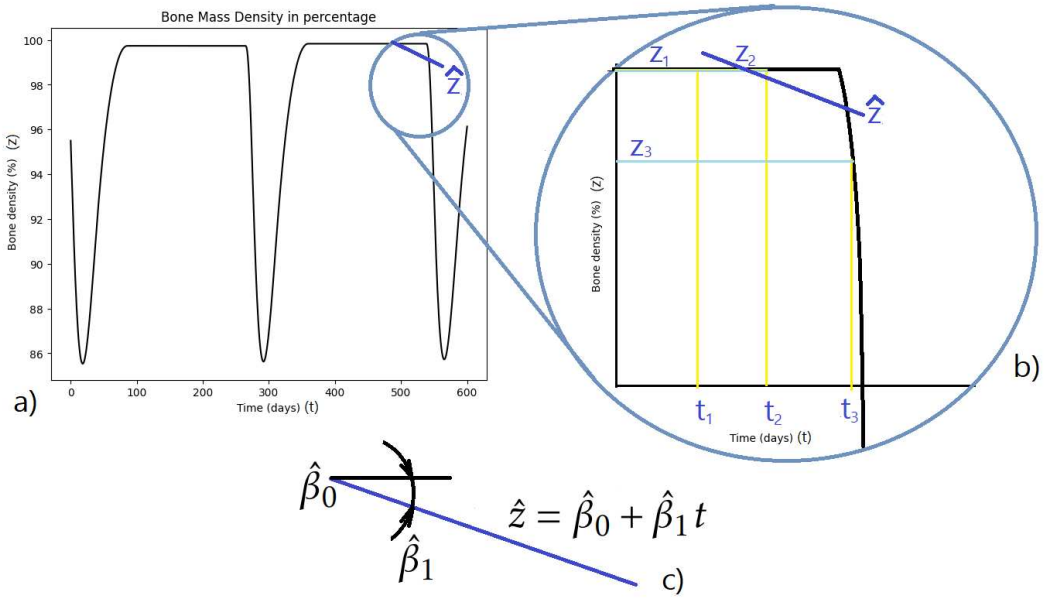

Figure 3: a) Bone mass percentage (z) curve along the time t. b) Zoom of one portion of the graph described in a), where it was taken three ($r = 3$) points (in yellow (t-coordinates) and blue (z-coordinates)) for making a linear interpolation $\hat{z}$ (in blue). c) Zoom of the graph in b), where it is shown $\hat{\beta}_0$ and $\hat{\beta}_1$, which is the slope of $\hat{z}$-graph.

2.2 Biological model

From the biological perspective, the model for the bone remodeling process is formulated employing four coupled nonlinear differential equations acting over a state vector given as $\mathbf{s}_{BMU} = [s_0, s_1, s_2, z]^T(\mathbf{x}, t)$, corresponding to osteocytes, osteoclasts, osteoblasts, and bone (depending on material point $\mathbf{x}$ and time t), respectively, as detailed in Equation (10), which have some similarities with Komarova's model framework (see Komarova et al. [29]).

$$\begin{cases} \dfrac{ds_0}{dt} = \alpha_0 s_0^{g_{00}} x_1^{g_{10}} s_2^{g_{20}} - \beta_0 s_0 & \text{(10a)} \\ \dfrac{ds_1}{dt} = C_{BMU}\alpha_1 s_0^{g_{01}} s_1^{g_{11}} s_2^{g_{21}} - \beta_1 s_1 & \text{(10b)} \\ \dfrac{ds_2}{dt} = C_{BMU}\alpha_2 s_0^{g_{02}} s_1^{g_{12}} s_2^{g_{22}} - \beta_2 s_2 & \text{(10c)} \\ \dfrac{dz}{dt} = k_0 y_0 - k_1 y_1 + k_2 y_2 & \text{(10d)} \end{cases}$$

where g_{ij} is the paracrine factor on the cell j due to the presence of i-cell, and z is the bone mass percentage, that has into account the difference between the number of osteoclasts/osteoblasts and its steady state (named $\overline{s_i}$), i.e. $2y_i = (s_i - \overline{s_i}) + |(s_i - \overline{s_i})|$ [23, 43, 44]. We have formulated the equations for osteocytes in the manner denoted as 10a, endeavoring to emulate a format akin to that utilized in equations 10b and 10c presented by Komarova et al. [29] However, the coefficients g_{i0} indeed exhibit a null dependency on osteoblasts and osteoclasts, see table 1. In addition, C_{BMU} is a coupling factor that considers the recruitment and integration as a unity of the BMU's cells through the master cell called osteocyte, given by

$$C_{BMU} = \begin{cases} c & \text{if } \dfrac{U}{U_{ref}} s_0 > W \\ 0 & \text{Otherwise} \end{cases} \tag{11}$$

In this equation, c represents a constant that accounts for the level of integration and functioning of the Basic Multicellular Unit (BMU). The mechanical energy density is denoted as U, and U_{ref} serves as a reference value to determine if the mechanical loading is sufficient to maintain the BMU as a unit. The biochemical paracrine factor g_{ij} captures the influence of cell i on cell j [29, 43, 44]. Additionally, W represents the energy density threshold at which the BMU can sustain its functionality.

The coefficients α_i and β_i can be analyzed in different scenarios, considering various combinations of biological damage and mechanical effects.

The equation for bone mass percentage (z) determines the difference between the number of osteoclasts and osteoblasts and its steady state, denoted as $\overline{x}_i$, which is obtained by solving $\frac{d\mathbf{s}_{BMU}}{dt} = 0$. This enables the computation of the bone mass percentage present in the bone.

Moreover, in equation 10d, the term of y_0 of bone mass formation is supported due to the role of osteocytes in the bone mass formation. Hence, contrary to the findings of Cresswell et al. [14], who suggested a limited role of osteocytes in this process, studies by Komori [30], O'Brien et al. [37], and Sims and Vrahnas [49] have highlighted a more active role of osteocytes in bone formation. Komori [30] particularly underscores the complexity of the osteocyte network in regulating bone mass, which encompasses bone formation and resorption. This dual functionality is essential for understanding how osteocytes can significantly influence bone mass. Further supporting this notion, O'Brien et al. [37] demonstrated the critical impact of PTHR1 signaling in osteocytes, which leads to increased bone mass and remodeling. This pathway involves the suppression of SOST/Sclerostin and activating LRP5 signaling, which is crucial for elevating osteoblast numbers and, consequently, bone mass. Additionally, studies have shown that PTH directly affects osteocytes, with the suppression of sclerostin expression playing a vital role in osteoblastogenesis [49]. These findings underscore osteocytes' significant and active role in bone mass formation, mediated through complex signaling pathways regulating bone metabolism. Therefore, utilizing the information provided by [37], this article has employed the experimental fact that osteocytes have two lines of action to generate bone mass: via BMU signaling, increasing the dynamic activity of osteoblasts and osteoclasts, but also they can increase bone mass (without involving osteoclasts in a remodeling process) by giving specific signals to osteoblasts to carry out bone mass apposition from local stimuli, such as mechanical loads. Also, in the presence of low mechanical loads, osteocytes can undergo apoptosis, which decreases bone mass in their environment. Therefore, equation 10d, which displays the evolution of bone mass over time, incorporates the coupling of the BMU in the remodeling process and its oscillatory effect on remodeling (second and third terms on the right-hand side of the equation). It also accounts for the effect of mechanical loading, which can lead to apoptosis or the generation of mass by osteoblasts, represented by the first term on the right-hand side.

In addition, it is posited that osteocytes may generate signals conducive to incorporating a greater number of osteocytes into their network, thereby facilitating the perception of mechanical conditions within their environment. For this reason, the recruitment of novel osteocytes has been permitted to depend on their own lineage, thereby fostering the establishment of an osteocyte network proficient in discerning mechanical cues, particularly in locales necessitating augmented bone formation, and subsequently diminishing in areas where it is no longer required. Therefore, In states of high mechanical demand, more osteoblasts may be recruited (via osteocytes), and some of these osteoblasts may transition into osteocytes as they become encased within the bone matrix. Consequently, it has been postulated that mechanical loading may indirectly affect the number of osteocytes through its influence on osteoblasts.

2.2.1 Osteocytes

Osteocytes play a vital role in bone tissue, constituting approximately 90% to 95% of the cellular component [48]. Originating from the osteoblast lineage, these cells reside within the bone matrix and adopt a dendritic morphology, establishing spatial connections with other osteocytes and neighboring osteoclasts, osteoblasts, and blood cells. Through their dendritic configuration and the network known as the Basic Multicellular Unit (BMU), osteocytes function as sensory cells, detecting external influences such as mechanical and metabolic factors and dynamically regulating bone response over time.

The significance of osteocytes in bone physiology has been highlighted by recent research. Schaffler and Kennedy [48] emphasized the role of osteocytes in the production of key bone proteins including osteoprotegerin (OPG), receptor activator of nuclear factor ligand (RANKL), and matrix extracellular phosphoglycoprotein (MEPE), among others. These proteins facilitate communication with osteoblasts, regulating the processes of mineralization and resorption mediated by osteoclasts. Thus, osteocytes sense mechanical loading and utilize this information to communicate with osteoclasts, promoting bone resorption, and coordinate with osteoblasts to drive bone formation.

Equation 10a describes the temporal evolution of osteocytes, indicating that the number of osteocytes present at a given "material point" depends on the mechanical loading, as reflected by the mechanical energy compared to a reference value, which can be written as follows:

$$\alpha_0 = k \cdot f_D \cdot \frac{U}{U_{ref}}, \tag{12}$$

where k is a factor that determines how many osteocytes can be in the bone matrix per time depending on the mechanical loading factor $\frac{U}{U_{ref}}$. If $\frac{U}{U_{ref}} > 1$, the number of osteocytes will grow due to the mechanical requirement; on the contrary, it will decrease because it is unnecessary to maintain bone tissue at low stresses; when this ratio is unity, the number of cells will be held. Also, f_D is a damage factor determining the limits where the osteocyte can survive and work (integrating the osteoclasts and osteoblasts) into the BMU, this factor is given by

$$f_D = \begin{cases} f & \text{if } \hat{D}(\mathbf{x}, t, \hat{\beta}_1) < d \\ 0 & \text{Otherwise} \end{cases} \tag{13}$$

where d is the limit of damage allowed before the BMU collapse. For its part, the factor β_0 is a parameter that considers the elimination rate of osteocytes, which is given by

$$\beta_0 s_0 = k. \tag{14}$$

According to Schaffler [48], osteocytes possess the ability to sense the mechanical environment and transmit biochemical signals to osteoclasts and osteoblasts. However, the reverse communication from osteoclasts/osteoblasts to osteocytes is less likely to occur. Furthermore, in instances where osteocytes undergo apoptosis, triggered by factors such as microfractures, glucocorticoids, estrogen loss, or immobilization, the remaining osteocytes respond by increasing the production of RANKL to stimulate the activation of new cells [5, 24, 48]. Hence, the factor g_{00} accounts for the communication among osteocytes. It is worth noting that by setting g_{10} and g_{20} as null values, the osteocyte model can align with the bone remodeling models proposed by Weinans et al. [54, 55], Jacobs et al. [27], Nackenhorst [36], and Huiskes et al. [25].

3 Computational model

The computational implementation of the aforementioned model is evaluated by employing it in a benchmark problem established in previous works [22, 23, 54, 55]. This section presents a detailed account of the computational procedure used to implement the model, including the geometry specifications, boundary conditions, and initial conditions. The section concludes with a comprehensive overview of the parameters utilized in the computational model.

3.1 Computational Procedure

Figure 4 illustrates the algorithm representing the model, as previously discussed. The implementation of the model will utilize the Finite Element Method. The algorithm is structured into two distinct sections: mechanics and biology. From a biological perspective, ordinary differential equations govern the representation of osteocytes, osteoclasts, osteoblasts, and bone mass, which evolve over time within each element. Osteocytes play a crucial role in maintaining the proper functioning of the entire Bone Multicellular Unit (BMU). According to [17], the evolution of different BMUs (corresponding to different elements) does not occur simultaneously within the bone remodeling cycle. In fact, if all cycles across material points were synchronized, the bone could experience weakness during certain periods while demonstrating strength at others. Consequently, it becomes necessary to initiate each element of the problem at distinct time points to prevent oscillation in the mechanical properties of the entire structure. This means that each element begins its BMU activity at varying moments until all elements activate their BMUs. The yellow box in Figure 4 symbolizes this biological activation, where the initial conditions initiate the biological process of each element at different moments. The mechanical process commences once the Bone Multicellular Units (BMUs) enter the bone remodeling cycle within each finite element of the mesh. The mechanical stress, strain, energy, and accumulated microdamage resulting from mechanical stresses are calculated within each finite element. Osteocytes act as sensors for damage and energy, integrating and preserving the BMU in areas where bone mass is required, thus ensuring proper functioning. Conversely, the BMU is removed from locations experiencing low mechanical loading, induced external damage (such as fractures or high-stress peaks), or biological factors

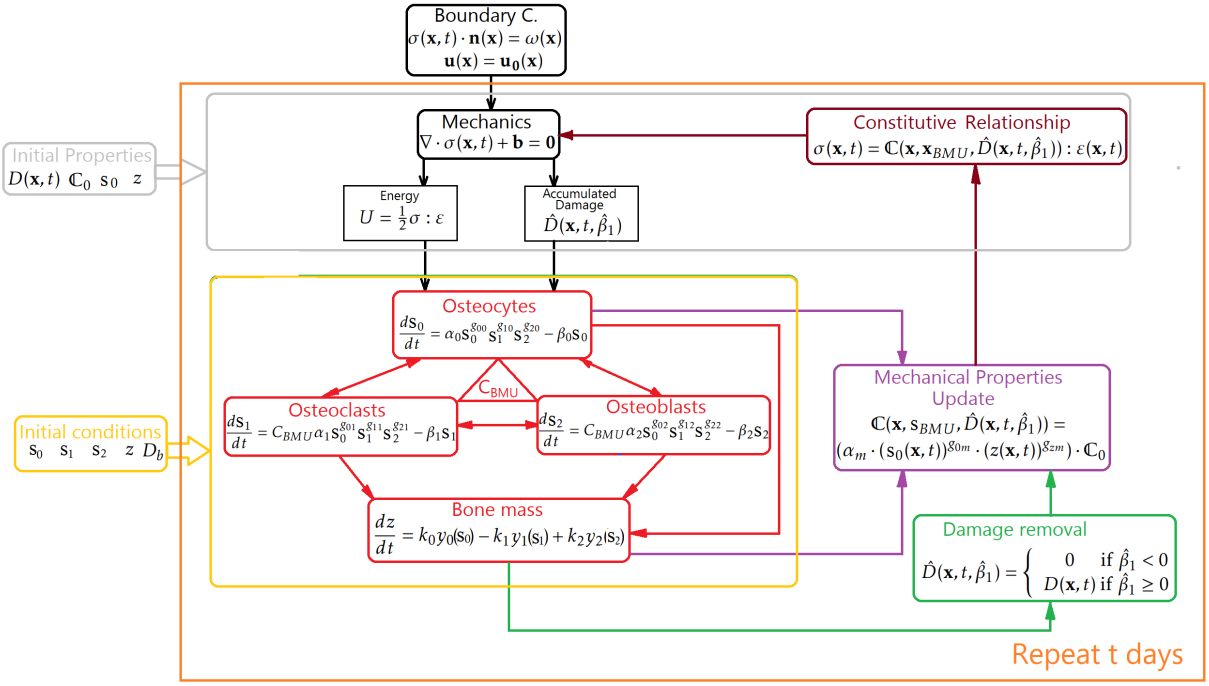

Figure 4: The sub-algorithm responsible for cell evolution, involving osteocytes, osteoclasts, osteoblasts, and bone mass, is enclosed within the yellow box. The mechanics, which receive updates of mechanical properties from both the bone mass and osteocytes (cells responsible for stress and strain sensing), are encapsulated within the gray box. The algorithm within the orange box represents the iterative process repeated over t days. The process initiates with the evolution of cells, and once all cells are active (at different random times), the mechanics come into play, functioning accordingly.

that disrupt normal osteoclasts or osteoblasts' functioning. The parameters C_{BMU} and x_0 play a crucial role in integrating and maintaining the BMU based on the mechanical energy within the finite element. When these parameters reach null values, the BMU ceases to function, and the cells lose their coordinated unit-like behavior, reducing mass.

The osteocyte plays a critical role in sensing mechanical stresses and subsequently adjusting the mechanical properties of each element, which are also influenced by the bone mass. Furthermore, the bone mass can accumulate microdamage caused by mechanical stresses, but this damage is typically repaired during each physiological cycle. However, if an abnormal cell cycle occurs, microdamage may accumulate unchecked, potentially leading to the disintegration of the BMU. The updated mechanical properties serve as the basis for establishing the constitutive relationship at the start of each new step, typically corresponding to one day.

The activation of all BMUs in the mesh takes place within a span of 1000 days, while the calculation of mechanical and biological events extends over a duration of 5000 days (total simulation of 6000 days). The mechanical processes are computed once every finite element has an active BMU.

The mechanics model was resolved by employing finite element methods, utilizing the precision of bilinear quadrilateral elements. Within each element, the ordinary differential equations were addressed using a 4th-order Runge-Kutta method. At every step of the computation, where the time increment is set to $\Delta t = 1$ day, the algorithm calculates the evolution of each cell within the Bone Modeling Units (BMUs). Once the computation is complete, the algorithm seamlessly updates the mechanical properties and handles the momentum equation adeptly. To ensure the accuracy of the simulation, previous numerical studies were conducted to determine the optimal value of Δt, as explored in the comprehensive work by Ramtani et al. [44]. Additionally, careful attention was given to selecting the appropriate element size, with a refined choice of $h = 2$ mm, as elucidated in the research conducted by Garzon et al. [23].

3.2 Geometry and boundary conditions

The geometric model employed in bone remodeling simulations typically adopts a simplified two-dimensional configuration, enabling efficient computational analysis while preserving essential morphological features. For instance, Xinghua et al. [60] utilized a 2D representation of a vertebral cross-section derived from radiographic measurements, discretized with a structured mesh of four-node bilinear finite elements. This approach allowed the modeling of both cortical and cancellous bone regions, reflecting anatomical variability across growth stages.

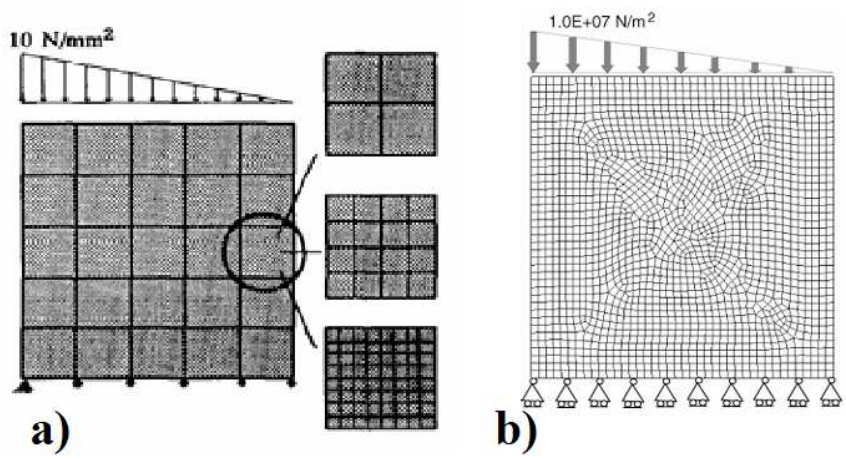

Figure 5: Benchmark geometries commonly used in bone remodeling simulations. (a) Structured mesh configuration from Weinans et al. [54]. (b) Unstructured mesh configuration from Chen et al. [10]. Both are representative models for testing algorithmic stability and spatial discretization effects.

The external contour of the vertebra was included in the simulation domain, enabling the prediction of shape evolution alongside density distribution.

Similarly, Weinans et al. [54] and Chen et al. [10] employed square plate models subjected to non-uniform compressive loading as a geometric abstraction to analyze remodeling behavior under mechanical stimuli. These geometries, although idealized, provide a controllable platform for systematically evaluating the effects of spatial discretization, boundary conditions, and mechanical load paths. The adoption of structured and unstructured meshes in these studies ensured compatibility with element-based and node-based finite element schemes, facilitating the implementation of density evolution algorithms over time. Figure 5 illustrates two classical benchmark examples commonly used in the study of bone remodeling algorithms. Subfigure (a), adapted from [54], features a structured finite element mesh applied to a square plate under non-uniform loading. Subfigure (b), from [10], employs an unstructured mesh configuration. These benchmark cases are widely recognized as scenarios for evaluating the performance and stability of numerical approaches in computational bone remodeling.

Figure 6 showcases the geometry and boundary conditions employed to examine the strengths and weaknesses of the aforementioned model and algorithm. This geometry has been extensively employed in prior studies [10, 22, 54, 60], serving as a foundation for solving and comparing bone remodeling models, as well as exploring their capacity to resemble tree-like structures.

For this investigation, a square with a width of 0.1 m (equivalent to 10 cm) was utilized, comprising 2500 elements and 2601 nodes. A triangular distributed mechanical load was applied to the upper side. In contrast, the bottom side had constraints in the y-direction, except in the right corner, where a total displacement constraint was imposed. These parameters and conditions were selected to comprehensively analyze the model and algorithm's performance.

To ensure diverse initial conditions and avoid synchronicity among mesh elements during the bone remodeling cycle, we carefully selected random moments before 1000 days to define each mesh element's initial conditions for osteoclasts, osteoblasts, and bone mass. At the integration start time of $t = 1000$ days, we set the osteocytes, denoted as s_0, to initiate the Bone Multicellular Unit (BMU) integration process. Notably, the initial conditions for osteocytes, osteoclasts, osteoblasts, and bone mass percentage were set to $s_0 = 1.0$ cells, $s_1 = 11.58$ cells, $s_2 = 231.7$ cells, and $z = 95.5\%$, respectively, as reported in [23, 43, 44]. The number of osteocytes in the bone matrix is scaled by a factor of $\times 10^3$ to maintain biological plausibility by findings reported in the literature [12]. Thus, the reported value of osteocytes serves as a dimensional reference, reflecting both the influence of mechanical loading and the osteocyte dynamics in preceding stages.

To illustrate the results and monitor cell evolution within a single finite element, we specifically selected element number $e = 2215$, which falls within the identified BMU activated zone as depicted in Figure 6a).

By carefully defining initial conditions, tracking cell evolution in a specific element, we aimed to capture the intricate dynamics of bone remodeling and gain insights into the effects of induced and biological damage on the system.

We present three additional cases corresponding to Examples 2, 3, and 4 of the reference study (see Reference [60] and [42]). Each example models a 2D beam structure using quadrilateral finite elements, aiming to evaluate the effectiveness of a bone remodeling algorithm under different mechanical loading conditions. The remodeling process is simulated by optimizing the material distribution in response to mechanical stimuli, mimicking the adaptive behavior of bone tissue.

Examples 2 and 3 use an elongated beam oriented in the X-direction. A distributed compressive load is applied to the upper surface in both cases. In Example 2, the triangular load is concentrated toward the ends of the beam,

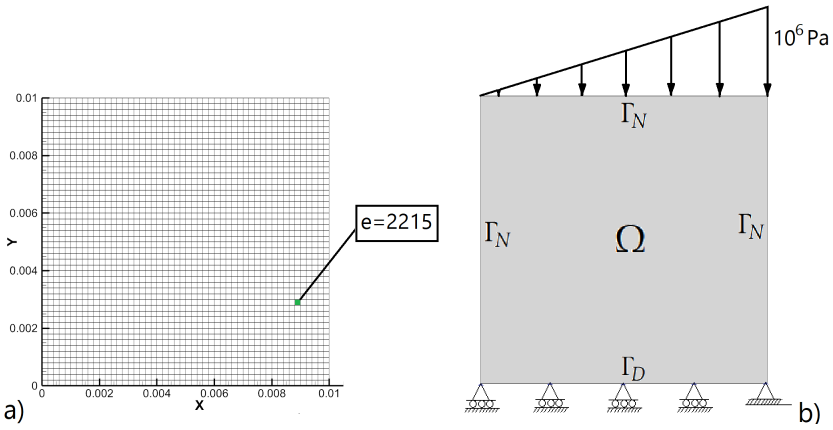

Figure 6: The square model itself has a size of 10 cm. The aforementioned details provide crucial insights into the mesh configuration and boundary conditions. a) Mesh utilized in the first example, dimensions given in meters (m), also, it is shown the element where we follow the dynamics of each BMU, i.e. element 2215 ($e = 2215$). b) The boundary conditions were imposed to ensure a benchmark example [23, 54]. The upper side of the square model, subjected to a triangular loading distribution as shown in the figure, experienced a maximum stress of 10^6 Pa.

resulting in lower loading in the central region. In Example 3, the load distribution is reversed—higher in the center and lower at the ends. These load configurations are based on those used by [60], in a similar remodeling context and are designed to demonstrate how different spatial load patterns influence the final optimized internal structure. The simulations provide insight into the redistribution of material in response to stress gradients, consistent with known bone remodeling patterns.

Example 4 involves a cantilever beam with a length in the X-direction that is three times its height in the Y-direction (see reference [42]). A single vertical point load is applied at the free end of the beam. This is a classical reference case in structural mechanics and serves to evaluate the ability of the remodeling model to predict optimal support structures under localized loading. The behavior observed in this example is consistent with the remodeling behavior reported by Quexada [42] in his work on structural adaptation.

All cases were discretized using finite quadrilateral elements. The total number of elements used was 2500, and the number of simulation steps (or iterations) was 6000. The mesh layout, loading conditions, and results for each example are shown in Figure 7. The remodeling process was iterated until convergence, defined as a stable material distribution representing a steady-state structural adaptation.

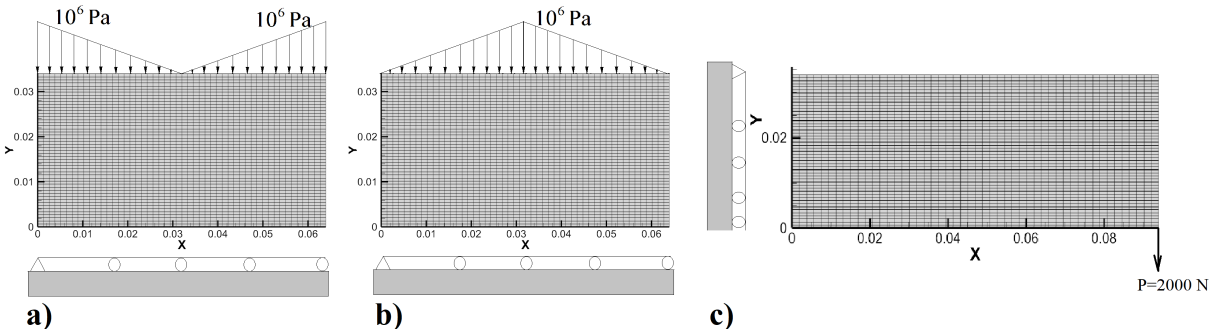

Figure 7: Load configurations and geometries used in Examples 2, 3, and 4. a) Example 2: elongated beam with triangular compressive load concentrated at the ends. b) Example 3: triangular load concentrated at the center. c) Example 4: cantilever beam with a point load at the free end. All models are discretized with quadrilateral finite elements to simulate bone remodeling through material redistribution. The boundary conditions are shown on the figure's side. In c) the mechanical load is $P = 2000N$, the size of the geometries are in the figure (in m).

3.3 Parameters

We have extracted the relevant physiological bone remodeling parameters from the notable sources [23, 29, 43, 44, 54], which are widely recognized in the field. These parameters play a crucial role in understanding and analyzing

the intricate process of bone remodeling. To facilitate comprehension and provide a comprehensive overview, we have organized and presented these parameters in a convenient tabular format, as demonstrated in Table 1. This table is a reference for researchers, clinicians, and professionals studying and evaluating bone remodeling dynamics. Most of the parameters have been extracted from literature as shown in the table, and others were obtained from this research using a sensitivity analysis.

Table 1: Parameters used in this work.Parameters with explicit references were obtained from previously published literature. Parameters without citations were determined via a trial-and-error approach, aiming to ensure the numerical stability of the model and the convergence of its mathematical and computational formulation.

Parameter	Action	Value
Mechanical Parameters		
E	Young Modulus	64 MPa [23, 54, 55]
ν	Poisson Modulus	0.3 [23, 54, 55]
U_{ref}	Reference energy	800 Pa [23, 54, 55]
g_{0m}	osteocyte-derived paracrine regulation	2 [23, 54, 55]
g_{zm}	bone mass-derived strenght material constant	0
θ	level of damage accumulation	0.01 $MPa^{-1} \cdot days^{-1}$
r	Number of points for sensing bone mass	3
General Biological Parameters		
c	BMU integration	1.0
W	BMU energy activation	0.50
k	Osteocyte production rate	0.3125 $days^{-1}$ [23, 54, 55]
g_{00}	osteocyte autocrine regulation	1 [23, 54, 55]
g_{10}	osteoclast-derived paracrine regulation	0
g_{20}	osteoblast-derived paracrine regulation	0
f	Damage factor on osteocytes	1
d	Damage limit factor before collapse	0.4
α_1	Osteoclast production rate	3 osteoblasts .day^{-1} [29]
α_2	Osteoblast production rate	4 osteoblasts .day^{-1} [29]
β_1	Osteoclast removal rate	0.2 osteoclasts .day^{-1} [29]
β_2	Osteoblast removal rate	0.02 osteoclasts .day^{-1} [29]
g_{01}	osteocyte-derived paracrine regulation	0
g_{11}	osteoclast autocrine regulation	1.1[29]
g_{21}	osteoblast-derived paracrine regulation	-0.5[29]
g_{02}	osteocyte-derived paracrine regulation	0
g_{12}	osteoclast-derived paracrine regulation	1[29]
g_{22}	osteoblast autocrine regulation	0[29]
k_0	Normalized activities of bone formation/resorption	1.0 % osteocytes^{-1} day^{-1}
k_1	Normalized activities of bone resorption	0.093 % osteoclasts^{-1}day^{-1}[29]
k_2	Normalized activities of bone formation	0.0008 % osteoblasts^{-1}day^{-1}[29]

3.4 Computational cases

We comprehensively analyzed the model's capabilities, utilizing the geometric configuration depicted in Figure 6 and figures 7. The study involved one primary simulation that can give us information about the dynamical evolution of osteoclasts, osteoblasts, osteocytes, bone mass, and micro-damage.

Our simulations were conducted in an undamaged domain, providing a baseline for comparison. Secondly, in the second part of this paper, we introduced induced damage directly into the designated region illustrated, where the damage function $D(\mathbf{x}, t)$ was set to 1.0. This allowed us to evaluate the model's response to explicit mechanical damage.

Regarding parameter sensitivity, prior works such as that of Komarova et al. [29] have delved into stability analyses, elucidating parameter ranges within the remodeling model. Furthermore, as an extension of this endeavor, Ramtani et al. [43] explored a set of rules governing parameters within a biologically plausible range. The

present study exclusively focuses on the remodeling model incorporating Basic Multicellular Units (BMUs) and osteocytes, harmonizing cellular behavior with mechanical phenomena within the continuous medium.

4 Results and discussion

Figure 8 presents the $2D$ visualizations of the aforementioned model, showcasing the results obtained. The first column corresponds to $t = 1000$ days, representing the time when the model is fully coupled to obtain the Bone Multicellular Unit (BMU) associated with each element. By employing a color code, it is evident that the cells within each finite element are not synchronized, indicating that they are at different stages of the bone remodeling cycle. This asynchrony is crucial for maintaining the structural integrity of the bone.

Columns b), c), and d) in Figure 8 correspond to $t = 1700$, $t = 3400$, and $t = 5000$ days, respectively. In the first and second rows (osteoclasts and osteoblasts), black points represent cells at the peak of their bone remodeling cycle, while white points represent cells at the bottom part of the cycle, with the lower values. The third column showcases the osteocytes responsible for constructing and recruiting the BMU in response to mechanical loads. These osteocytes strategically reinforce the bone in areas where it is necessary to withstand external loads, as illustrated in the other three rows (first, second, and fourth). The results exhibit a tree-like structure, which optimally preserves the structural integrity of the bone and enhances its ability to support external loads.

Figure 9 offers a detailed examination of a specific element indicated in 6a). Within this element, we can track the dynamics of osteoclasts, osteoblasts, bone mass density, and the percentage of damage. The final graph illustrates the gradual removal of damage throughout the simulation, depicting the process of bone renewal and restoration of its integrity.

An important assumption in the present model is the adoption of a linear and homogeneous mechanical framework for describing bone tissue behavior. This assumption implies that the stress-strain relationship follows Hooke's law and that the mechanical properties of the material are uniformly distributed across the domain. While this simplification omits the known anisotropy and heterogeneity of bone at the microscale, it enables a tractable integration of mechanical and biological components within the finite element context. The linear elasticity assumption has been widely adopted in foundational models of bone adaptation, including those by Weinans et al. [54] and Huiskes et al. [25], where it has proven sufficient for capturing the long-term effects of mechanical stimuli on density evolution [25, 54] It is particularly appropriate for physiological loading regimes, where bone generally remains within the elastic range. Although more complex material models could capture non-linear responses or damage accumulation more precisely, such enhancements often come at the cost of increased computational complexity and reduced interpretability. Homogeneity, as implemented in this model, is applied at the tissue scale and not at the cellular or microstructural level. While this does not account for local variations in mineralization, porosity, or lamellar organization, our model allows for emergent heterogeneity by coupling mechanical signals to biological responses. In particular, the local mechanical properties are dynamically updated based on the activity of osteocytes, osteoclasts, and osteoblasts, allowing the tissue to adapt its mechanical competence in response to both loading and damage. Future extensions of this model could relax these assumptions by introducing spatially variable material properties or nonlinear constitutive laws, particularly for studying high-stress regimes, anisotropic structures, or failure mechanisms. Nonetheless, for the purposes of simulating physiological bone remodeling and mechanobiological feedback, the linear and homogeneous approach provides a robust and computationally efficient foundation.

It is worth noting that the simulations presented in Figure 9 correspond to element $e = 2215$, which does not experience structural collapse, as the damage remains below 20% throughout the remodeling cycle. The apparent increase in bone mass slightly above 100% is a result of minor numerical accumulation errors, consistent with findings reported in Komarova et al. [29] and Garzón-Alvarado and Linero [23]. This small overestimation (typically between 0–4%) arises from the numerical integration of a large number of BMUs across the domain. Additionally, previous simulations have shown that such behavior may emerge even in healthy tissue because of the model's sensitivity to spatial and temporal discretization.

It is also important to compare with previous models in literature. The models—developed by Xinghua et al. [60], Weinans et al. [54], and Chen et al. [10]—share a common foundation: they simulate bone remodeling as a response to mechanical stimuli such as strain energy density. Figure 10 illustrates the typical outcomes from these approaches. Subfigure (a) displays a structured mesh with branching trabecular patterns, highlighting the mechanical adaptation simulated in [10]. In contrast, subfigure (b) reveals the checkerboard artifact observed in element-based simulations, where density is evaluated per element without ensuring continuity. Subfigure (c) improves upon this by adopting a node-based density update, resulting in a smoother, more physiological distribution, as proposed by [54].

These classical models primarily use simplified 2D geometries and scalar density fields to characterize bone adaptation. Their numerical outputs, as seen in the figure, focus on the evolution of bone density under fixed or variable loads. They capture essential mechanical phenomena but omit explicit biological regulators, such as osteocyte signaling or microdamage repair mechanisms. Moreover, the outputs are highly sensitive to mesh topology and integration methods, making numerical stability a key concern.

In contrast, our approach introduces a biologically enriched framework where bone remodeling is driven not only by mechanical stimuli but also by cellular dynamics. Unlike the classical approaches shown in Figure 10

c), the recent model incorporates asynchronous BMU activation, osteocyte sensing, and microdamage-triggered repair. While not illustrated in this figure, the new model generates remodeling patterns that are spatially heterogeneous and biologically plausible, including anisotropic trabecular formation. This level of detail provides a more comprehensive simulation of bone remodeling, bridging the gap between biomechanics and physiology.

The outcomes of the second set of simulations are summarized in Figure 11, structured as a matrix of four rows and three columns. Each column represents a distinct mechanical loading scenario, while the rows show the spatial distribution and activity of key components involved in bone remodeling: osteoclasts (row a), osteoblasts (row b), osteocytes (row c), and normalized bone mass (row d), expressed as a percentage of the maximum bone density (100%).

The example 2 simulates a beam under a distributed load applied along its upper surface, with peak intensities located at both ends. The internal bone architecture responds by forming a highly organized reticulated structure, with column-like struts and aligned trabeculae that resemble load paths in civil engineering structures such as bridges.

In row (a), osteoclasts appear in discrete zones, participating in the resorption of bone material where mechanical demand is minimal. Row (b) shows osteoblasts predominantly located in high-stress regions, depositing new bone to reinforce the structure. Row (c) illustrates the presence of osteocytes embedded throughout the bone matrix, particularly in regions subjected to sustained load, where they regulate remodeling via mechanosensing. Finally, row (d) shows the normalized distribution of bone mass, which closely follows the mechanical load paths, confirming that bone is preferentially deposited where it is structurally most necessary.

In example 3, we have applied a distributed load with its maximum intensity located centrally along the beam. This loading pattern is biomechanically relevant to scenarios such as vertebral load-bearing, where axial loads concentrate near the center.

The simulation reveals a strong centralization of cellular activity and bone mass. Osteoclasts (row a) are active at the periphery, resorbing material in low-stress zones. Osteoblasts (row b) concentrate in the central area, forming new bone in response to the increased mechanical demand. Osteocytes (row c) are denser in the mid-region, reflecting their role in detecting and integrating mechanical signals. The resulting bone mass distribution (row d) shows increased density in the center and tapering toward the ends, consistent with structural optimization principles.

The fourth example represents a cantilever beam fixed at the left end and subjected to a downward point load at the free right end—analogous to anatomical structures such as long bones under bending loads or spinal processes.

The simulation yields a bone structure resembling that of a mechanical beam, with increased bone mass along the tension side. The final bone mass pattern (row d) reflects an efficient load-bearing architecture, with optimized mass placement aligned with structural demands.

Across all examples, the remodeling process is governed by a coordinated interaction between the three cell types. Osteocytes, embedded within the mineralized matrix, sense mechanical stimuli and regulate the balance between osteoblast-mediated bone formation and osteoclast-mediated bone resorption. The observed cellular behaviors and bone mass adaptations suggest that the remodeling process effectively acts as a biologically driven topological optimization mechanism.

The model not only captures the spatial patterns of bone formation and resorption, but also reproduces biomechanically plausible architectures, demonstrating that mechanical cues alone—when coupled with biologically inspired algorithms—can guide efficient tissue distribution. These results highlight the potential of this approach as both a predictor of bone density patterns and a computational tool for simulating the natural process of structural adaptation in bone.

5 Conclusion

This study introduces a novel framework for modeling the bone remodeling process, offering valuable insights into the intricate interplay between biological events and mechanical dynamics. While the current model does not explicitly incorporate a multiscale approach, it leverages the computation of Bone Modeling Unit (BMU) components over time, simulating a multiscale-like model that captures both the biological and mechanical aspects of bone remodeling. Comparisons can be drawn between the 2D model and previous studies conducted by [23, 54, 55], where a tree-like structure was formed. However, this new framework goes beyond structural formation and delves into the simultaneous progression of biological and mechanical events.

One noteworthy aspect of this model is its ability to reproduce the temporal evolution of damage and the subsequent renewal of bone in each remodeling cycle. This represents a significant advancement, providing insights into how damage accumulates over time and how bone regeneration occurs in response.

It is important to remark, compared to classical models of bone remodeling—such as those based on Frost's mechanostat theory or the Komarova framework, which emphasize osteoclast and osteoblast dynamics—this model introduces a major conceptual shift by assigning a central regulatory role to osteocytes. Rather than treating these cells as passive mechanosensors or excluding them altogether, our approach positions them as active participants that coordinate remodeling through localized control of BMU activity. This allows for a more physiologically grounded simulation of how bone responds to mechanical demands and internal damage.

One of the main improvements over previous approaches is the introduction of a feedback mechanism based on the history of bone mass evolution. Most existing models rely on instantaneous thresholds to trigger bone resorption or formation based on mechanical inputs. In contrast, our use of a dynamic memory variable ($\hat{\beta_1}$) enables remodeling to be filtered over time. This better reflects the biological delay systems observed in vivo and reduces sensitivity to short-term fluctuations in load, which could otherwise result in unrealistic remodeling cycles. The model also addresses a key limitation of earlier frameworks: the assumption of synchronized remodeling across the tissue. Artificial synchronization can lead to unrealistic waves of bone turnover that do not match histological observations. Our model enables asynchronous BMU activation across spatial domains, which mimics the stochastic nature of bone remodeling in vivo and provides more realistic patterns of bone formation and resorption.

From a mechanical perspective, the model captures and explains the emergence of load-bearing structures such as tree-like trabecular geometries. These patterns are not imposed but arise from the local interaction between mechanical stress and biological feedback. This elevates the model beyond descriptive representation by offering a mechanistic explanation for architectural adaptation in bone under sustained mechanical loading. An additional novel feature is the prediction that osteocyte density may increase dynamically in response to sustained mechanical demand. This reflects the transition of osteoblasts into osteocytes in regions under load, effectively enhancing the sensing network. This mechanism could account for observed differences in osteocyte density across anatomical locations and life stages, which is rarely addressed in other models and opens new avenues for studying sensor network plasticity in bone. Another strength is the ability of the model to integrate biological, mechanical, and damage-related factors into a single coherent system. The osteocyte-regulated control loop supports targeted bone removal and deposition, depending on local mechanical conditions and internal microdamage. This stands in contrast to earlier approaches that attributed regulatory control to the tissue as a whole, rather than to specific cellular mechanisms.

An additional and significant conclusion derived from the implementation of this remodeling algorithm in this study is that the simulated bone remodeling process—driven by the orchestrated interaction between osteoclasts, osteoblasts, and osteocytes—not only replicates biological tissue adaptation but also effectively performs a form of topological optimization.

As demonstrated in the second set of examples (Figure 11), this biologically inspired remodeling model leads to the emergence of structures that closely resemble those generated by classical topological optimization algorithms used in structural engineering. In particular, the resulting material distributions maximize structural efficiency by increasing mass where loads are concentrated and minimizing it in unloaded regions.

Therefore, beyond its physiological relevance, our remodeling framework offers a powerful computational strategy to explore biomimetic design principles for structural optimization. It provides a biologically grounded alternative to conventional engineering methods, with the added benefit of simulating temporal evolution and adaptive repair mechanisms—features that are typically absent in purely mathematical optimization models.

This reinforces the notion that bone remodeling is not merely a regenerative process, but a natural, load-driven optimization algorithm evolved through biology. Its capacity to self-organize in response to functional demands holds promising implications for fields such as biomechanics, tissue engineering, and bioinspired structural design.

However, the model has limitations. It simplifies complex molecular signaling into aggregated parameters and does not yet include systemic hormonal influences, matrix deposition kinetics, or detailed bone anisotropy. While the finite element mesh captures spatial variability, it does so at the tissue scale, and more realistic cell distributions—such as heterogeneous populations of osteocytes, osteoblasts, and osteoclasts—are not yet fully incorporated. Despite these limitations, the model's modular architecture allows for future expansion. It can be extended to simulate pathological remodeling, aging, or mechanical damage, and to test the impact of therapies or surgical interventions. Its core structure, based on local control and emergent coordination, is generalizable and can be adapted to model other mechanically regulated tissues, including cartilage, tendon, and bone–tumor interactions.

In summary, this new framework presents a promising avenue for studying bone remodeling processes by integrating biological and mechanical events. Its ability to include diseases and investigate their impact on bone structure and mechanics opens up new possibilities for understanding the underlying mechanisms and developing potential interventions. This aspect will be shown in the second part of this research.

6 Declarations

6.1 Ethical Approval

This declaration is not applicable.

6.2 Competing interests

All authors declare no competing or finantial interest.

6.3 Authors' contributions

All author contributed to every stage of the research of this paper from conceptualization, through methodology, investigation, formal analysis, writing, editing, software reviewing and supervision.

6.4 Funding

This work was supported by Biotechnology Institute - Universidad Nacional de Colombia, Laboratoire CSPBAT, equipe LBPS, CNRS (UMR 7244),Universit e Sorbonne Paris Nord and Department of Mechanical Engineering,.

6.5 Availability of data and materials

The data obatined on the solution of these models can be accessed by sending an email to the corresponding author.

References

[1] Dulshara S. Amarasekara, Sumi Kim, and Jaerang Rho. Regulation of osteoblast differentiation by cytokine networks. *International Journal of Molecular Sciences*, 22(6):2851, 2021. doi: 10.3390/ijms22062851.

[2] M.T. Bahia, M.B. Hecke, E.G.F. Mercuri, and M.M. Pinheiro. A bone remodeling model governed by cellular micromechanics and physiologically based pharmacokinetics. *Journal of the Mechanical Behavior of Biomedical Materials*, 104:103657, 2020. doi: 10.1016/j.jmbbm.2020.103657.

[3] Sébastien Baiotto, Béatrice Labat, Laurence Vico, and Mustapha Zidi. Bone remodeling regulation under unloading conditions: Numerical investigations. *Computers in Biology and Medicine*, 39(1):46–52, 2009. doi: 10.1016/j.compbiomed.2008.10.008.

[4] G.S. Beaupré, T.E. Orr, and D.R. Carter. An approach for time-dependent bone modeling and remodeling application: a preliminary remodeling simulation. *J. Orthop. Res.*, 8 (5):662–670, 1990.

[5] L. Bonewald. "osteocytes". *In: Marcus R, editor. Osteoporosis. 3rd. Elsevier*, pages 170–189, 2008.

[6] Brendan F. Boyce and Lianping Xing. Functions of rankl/rank/opg in bone modeling and remodeling. *Archives of Biochemistry and Biophysics*, 473(2):139–146, 2008. doi: 10.1016/j.abb.2008.03.018.

[7] R.A. Brand. Biographical sketch: Julius wolff, 1836-1902. *Clin Orthop Relat Res.*, 468(4):1047–9, 2010.

[8] D Carter. Mechanical loading histories and cortical bone remodeling. *Calcif. Tissue Int.*, 36 (S1):19–24, 1984.

[9] Marine Cazenave, Anna Oettlé, Travis Rayne Pickering, Jason L. Heaton, Masato Nakatsukasa, J. Francis Thackeray, Jakobus Hoffman, and Roberto Macchiarelli. Trabecular organization of the proximal femur in paranthropus robustus: Implications for the assessment of its hip joint loading conditions. *Journal of Human Evolution*, 153:102964, 2021. ISSN 0047-2484. doi: https://doi.org/10.1016/j.jhevol.2021.102964. URL https://www.sciencedirect.com/science/article/pii/S0047248421000166.

[10] G. Chen, G. Pettet, M. Pearcy, and D. L. S. McElwain. Comparison of two numerical approaches for bone remodelling. *Medical Engineering & Physics*, 29(1):134–139, 2007.

[11] Benito M. Chen-Charpentier and Ibrahim Diakite. A mathematical model of bone remodeling with delays. *Journal of Computational and Applied Mathematics*, 291:76–84, 2016. doi: 10.1016/j.cam.2014.11.025.

[12] Man Huen Victoria Choy, Ronald Man Yeung Wong, Simon Kwoon Ho Chow, Meng Chen Li, Yu Ning Chim, Tsz Kiu Li, Wing Tung Ho, Jack Chun Yiu Cheng, and Wing Hoi Cheung. How much do we know about the role of osteocytes in different phases of fracture healing? a systematic review. *Journal of Orthopaedic Translation.*, 21:111–121, 2020.

[13] S. Cowin and D.H. Hegedus. Bone remodeling i: theory of adaptive elasticity. *J. Elasticity*, 6:313–326, 1976.

[14] E.N. Cresswell, T.M. Nguyen, M.W. Horsfield, A.J. Alepuz, T.A. Metzger, G.L. Niebur, and C.J. Hernandez. Mechanically induced bone formation is not sensitive to local osteocyte density in rat vertebral cancellous bone. *J Orthop Res.*, 36(2):672–681, 2018.

[15] K. Culmann. *Graphical Analysis of Roof Frameworks*. Springer, Zurich, 1866.

[16] K. Culmann. *Statistical Studies of the Force Paths in Supporting Structures*. Springer, Zurich, 1876.

[17] H.K. Datta, W.F. Ng, J.A. Walker, S.P. Tuck, and S.S. Varanasi. The cell biology of bone metabolism. *J Clin Pathol*, 61:577–587, 2008.

[18] J.R. Fernández, J.M. García-Aznar, and R. Martínez. Piezoelectricity could predict sites of formation/resorption in bone remodelling and modelling. *Journal of Theoretical Biology*, 292:86–92, 2012. doi: 10.1016/j.jtbi.2011.09.032.

[19] H. M. Frost. *Mathematical Elements of Lamellar Remodelling*. Charles C. Thomas, Springfield, 1964.

[20] H. M. Frost. Bone "mass" and the "mechanostat": a proposal. *Anat. Rec.*, 219(1):1–9, 1987.

[21] H. M. Frost. Skeletal structural adaptations to mechanical usage (satmu): 1. redefining wolff's law: the bone modeling problem. *Anat. Rec.*, 226(4):403–413, 1990.

[22] D. P. Fyhrie and M. B. Schaffler. The adaptation of bone apparent density to applied load. *Journal of Biomechanics*, 28(2):135–146, 1995.

[23] D. A. Garzón-Alvarado and D. Linero. Comparative analysis of numerical integration schemes of density equation for a computational model of bone remodelling. *Computer Methods in Biomechanics and Biomedical Engineering*, 15(11):1189–1196, 2012.

[24] G. Gu, M. Nars, T.A. Hentunen, K. Metsikkö, and H.K. Väänänen. Isolated primary osteocytes express functional gap junctions in vitro. *Cell Tissue Res*, 323(2):263–71, 2006.

[25] R. Huiskes, H. Weinans, H.J. Grootenboer, D. Dalstra, B. Fudala, and T.J. Slooff. Adaptive bone-remodeling theory applied to prosthetic-design analysis. *J. Biomech.*, 20 (11-12):1135–1150, 1987.

[26] Mengke Huo, Siyuan He, Yun Zhang, Yuxiao Feng, and Jian Lu. Simulation on bone remodeling with stochastic nature of adult and elderly using topology optimization algorithm. *Journal of Biomechanics*, 136:111078, 2022. doi: 10.1016/j.jbiomech.2022.111078.

[27] C.R. Jacobs, J.C. Simo, G.S. Beaupre, and D.C. Carter. Adaptive bone remodeling incorporating simultaneous density and anisotropy considerations. *J. Biomechanics*, 6:603–613, 1997.

[28] Julia S. Kenkre and John H.D. Bassett. The bone remodelling cycle. *Annals of Clinical Biochemistry*, 55(3): 308–327, 2018. doi: 10.1177/0004563218759371.

[29] Svetlana V Komarova, Robert J Smith, S Jeffrey Dixon, Stephen M Sims, and Lindi M Wahl. Mathematical model predicts a critical role for osteoclast autocrine regulation in the control of bone remodeling. *Bone*, 33 (2):206–215, 2003.

[30] T. Komori. Functions of the osteocyte network in the regulation of bone mass. *Cell Tissue Res.*, 352(2):191–8, 2013.

[31] Vincent Lemaire, Frank L. Tobin, Larry D. Greller, Carolyn R. Cho, and Larry J. Suva. Modeling the interactions between osteoblast and osteoclast activities in bone remodeling. *Journal of Theoretical Biology*, 229(3): 293–309, 2004. doi: 10.1016/j.jtbi.2004.03.023.

[32] P. Liò, E. Merelli, N. Paoletti, and M. Viceconti. A combined process algebraic and stochastic approach to bone remodeling. *Electronic Notes in Theoretical Computer Science*, 277:41–52, 2011. doi: 10.1016/j.entcs.2011.09.034.

[33] Basil Mathai, Santanu Dhara, and Sanjay Gupta. Bone remodelling in implanted proximal femur using topology optimization and parameterized cellular model. *Journal of the Mechanical Behavior of Biomedical Materials*, 125:104903, 2022. doi: 10.1016/j.jmbbm.2021.104903.

[34] L.M. McNamara, R.J. Majeska, S. Weinbaum, V. Friedrich, and M.B. Schaffler. Attachment of osteocyte cell processes to the bone matrix. *Anat Rec (Hoboken).*, 292(3):355–63, 2009.

[35] Adam Moroz and David Ian Wimpenny. Allosteric control model of bone remodelling containing periodical modes. *Biophysical Chemistry*, 127(3):194–212, 2007. doi: 10.1016/j.bpc.2007.02.001.

[36] U Nackenhorst. Numerical simulation of stress stimulated bone remodeling. *Technische Mechanik*, 17(1): 31–40, 1997.

[37] C.A. O'Brien, L.I. Plotkin, C. Galli, J.J. Goellner, A.R. Gortazar, M.R. Allen, A.G. Robling, M. Bouxsein, E. Schipani, C.H. Turner, R.L. Jilka, R.S. Weinstein, S.C. Manolagas, and T. Bellido. Control of bone mass and remodeling by pth receptor signaling in osteocytes. *PLoS One.*, 3(8):e2942, 2008.

[38] V.A. Papathanasopoulou, D.I. Fotiadis, G. Foutsitzi, and C.V. Massalas. A poroelastic bone model for internal remodeling. *International Journal of Engineering Science*, 40(5):511–530, 2002. doi: 10.1016/S0020-7225(01)00076-3.

[39] Maria-Ioana Pastrama, Stefan Scheiner, Peter Pivonka, and Christian Hellmich. A mathematical multiscale model of bone remodeling, accounting for pore space-specific mechanosensation. *Bone*, 107:208–221, 2018. doi: 10.1016/j.bone.2017.11.009.

[40] Marek Pawlikowski, Szymon Sikora, and Gustaw Ostrowski. The role of mathematical models in prediction of osteoarthritis development. *Computers in Biology and Medicine*, 193:110407, 2025. doi: 10.1016/j.compbiomed.2025.110407.

[41] Peter Pivonka, Pascal R. Buenzli, Stefan Scheiner, Christian Hellmich, and Colin R. Dunstan. The influence of bone surface availability in bone remodeling—a mathematical model including coupled geometrical and biomechanical regulations of bone cells. *Engineering Structures*, 47:134–147, 2013. doi: 10.1016/j.engstruct.2012.09.006.

[42] Diego Alfredo Quexada Rodríguez. Computational model of bone remodeling using discrete structures. https://repositorio.unal.edu.co/handle/unal/79884, 2021. Accessed: 2025-06-16.

[43] S. Ramtani, J.F. Sánchez, A. Boucetta, R. Kraft, J.J. Vaca-González, and D.A. Garzón-Alvarado. A coupled mathematical model between bone remodeling and tumors: a study of different scenarios using komarova's model. *Biomech Model Mechanobiol*, 2023.

[44] S. Ramtani, L. Toudji, A. Boucetta, T. Boukharouba, and D.A. Garzón-Alvarado. Komarova's bone remodeling type model revisited within the context of a new parameter affecting both production and removal activities of osteoblasts and osteoclasts. *Journal of Mechanics in Medicine and Biology*, 2023.

[45] R. Ruimerman, P. Hilbers, B. van Rietbergen, and R. Huiskes. A theoretical framework for strain-related trabecular bone maintenance and adaptation. *J Biomech*, 38(4):931–941, 2005.

[46] R. Ruimerman, B. Van Rietbergen, P. Hilbers, and R. Huiskes. The effects of trabecular-bone loading variables on the surface signaling potential for bone remodeling and adaptation. *Ann Biomed Eng.*, 33(1):71–8, 2005.

[47] B. Rüttimann. *A Noteworthy Meeting of the Society for Nature Research in Zurich Two Important Precursors of Julius Wolff: Carl Culmann and Hermann von Meyer*, pages 13–22. De Gruyter, Berlin, New York, 1992. ISBN 9783110875676. doi: doi:10.1515/9783110875676.13. URL https://doi.org/10.1515/9783110875676.13.

[48] M.B. Schaffler and O.D. Kennedy. Osteocyte signaling in bone. *Curr Osteoporos Rep*, 10(2):118–25, 2012.

[49] N.A. Sims and C. Vrahnas. Regulation of cortical and trabecular bone mass by communication between osteoblasts, osteocytes and osteoclasts. *Arch Biochem Biophys.*, 561:22–8, 2014.

[50] A.E. Tami, P. Nasser, O. Verborgt, M.B. Schaffler, and M.L. Knothe Tate. The role of interstitial fluid flow in the remodeling response to fatigue loading. *J Bone Miner Res.*, 17(11):2030–7, 2002.

[51] G. Von Meyer. *The Architecture of the Spongy Substance and the Formation of the Cancellous Bone Tissue*. F.C.W Vogel, Leipzig, 1867.

[52] G. Von Meyer. *Handbook of Systematic Human Anatomy*. F.C.W Vogel, Leipzig, 1875.

[53] Boyang Wan, Nobuhiro Yoda, Keke Zheng, Zhongpu Zhang, Chi Wu, Jonathan Clark, Keiichi Sasaki, Michael Swain, and Qing Li. On interaction between fatigue of reconstruction plate and time-dependent bone remodeling. *Journal of the Mechanical Behavior of Biomedical Materials*, 136:105483, 2022. doi: 10.1016/j.jmbbm.2022.105483.

[54] H. Weinans, R. Huiskes, and H.J. Grootenboer. The behavior of adaptive bone-remodeling: Simulation models. *J. Biomechanics*, 25(12):1425–1441, 1992.

[55] H. Weinans, R. Huiskes, and H.J. Grootenboer. Effects of fit and bonding characteristics of femoral stems on adaptive bone remodeling. *J. Biomechanical Engineering*, 116:393–400, 1994.

[56] J. Wolff. Ueber die innere architectur der knochen und ihre bedeutung für die frage vom knochenwachsthum. *Virchows Archiv Pathol Anat Physio.*, 50:389–450, 1870.

[57] J. Wolff. Zur lehre von der fracturenheilung. *Langenbecks Arch Klin Chir Ver Dtsch Z Chir*, 2:546–551, 1873.

[58] J. Wolff. Das gesetz der transformation der knochen. berlin, germany: Verlag von august hirschwald. *Dtsch Med Wochenschr*, 19(47):12222–1224, 1892.

[59] P. Wriggers. "contact kinematics". *in Computational Contact Mechanics, Springer Berlin.*, chapter 4:56–67, 2006.

[60] Z. Xinghua, G. He, Z. Dong, and G. Bingzhao. A study of the effect of non-linearities in the equation of bone remodeling. *Journal of Biomechanics*, 35(7):951–960, 2002.

[61] M. Zidi and S. Ramtani. Bone remodeling theory applied to the study of n unit-elements model. *Journal of Biomechanics*, 32(7):743–747, 1999. doi: 10.1016/S0021-9290(99)00033-0.

[62] Martin Zumsande, Dirk Stiefs, Stefan Siegmund, and Thilo Gross. General analysis of mathematical models for bone remodeling. *Bone*, 48(4):910–917, 2011. doi: 10.1016/j.bone.2010.12.010.

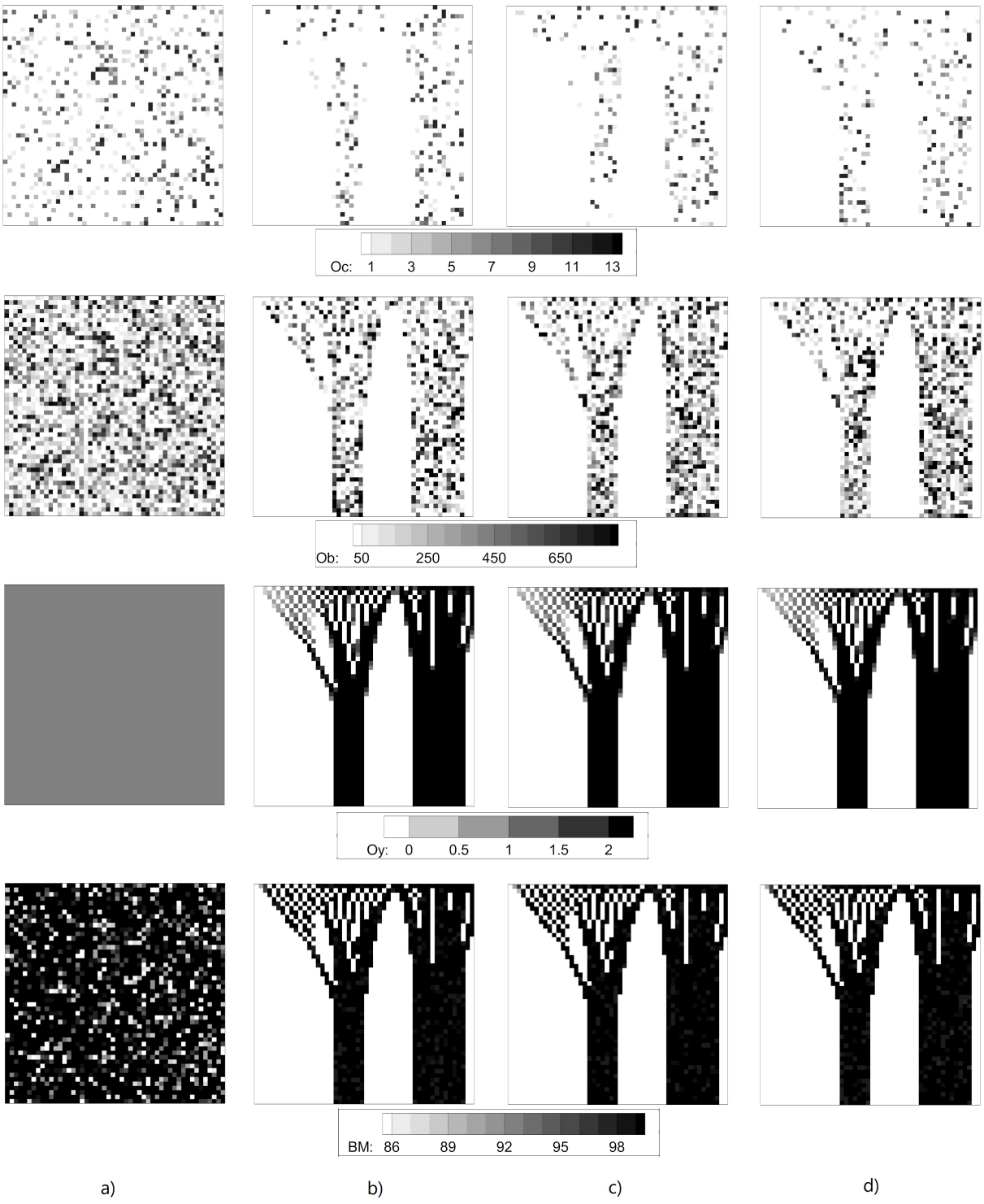

Figure 8: This figure presents the results of a physiological case, illustrating the bone remodeling process in $2D$ over time. The results are organized into four rows, representing different cell types and bone mass: the first row represents osteoclasts (OC) in terms of cell count; the second row represents osteoblasts (Ob) in terms of cell count; the third row represents osteocytes (Oy) in terms of cell count; and the fourth row represents bone mass (BM) in terms of percentage. The columns in Figure 8 correspond to different time points: a) The initial time, where all cells operate at different stages of the bone remodeling cycle, reflecting random initial conditions. b) Time = 1700 days, showcasing the progression of the bone remodeling process. c) Time = 3400 days, demonstrating further evolution and changes in the cell populations. d) Time = 5000 days, illustrating the later stages of the bone remodeling process. Prior to the initial time of coupling all cells in the remodeling process, the model incorporates 1000 steps (days) of Komarova's model without coupling with osteocytes and the damage process. These preliminary steps serve as a preparatory phase for the subsequent integration and interaction of the different cell types involved in the bone remodeling cycle.

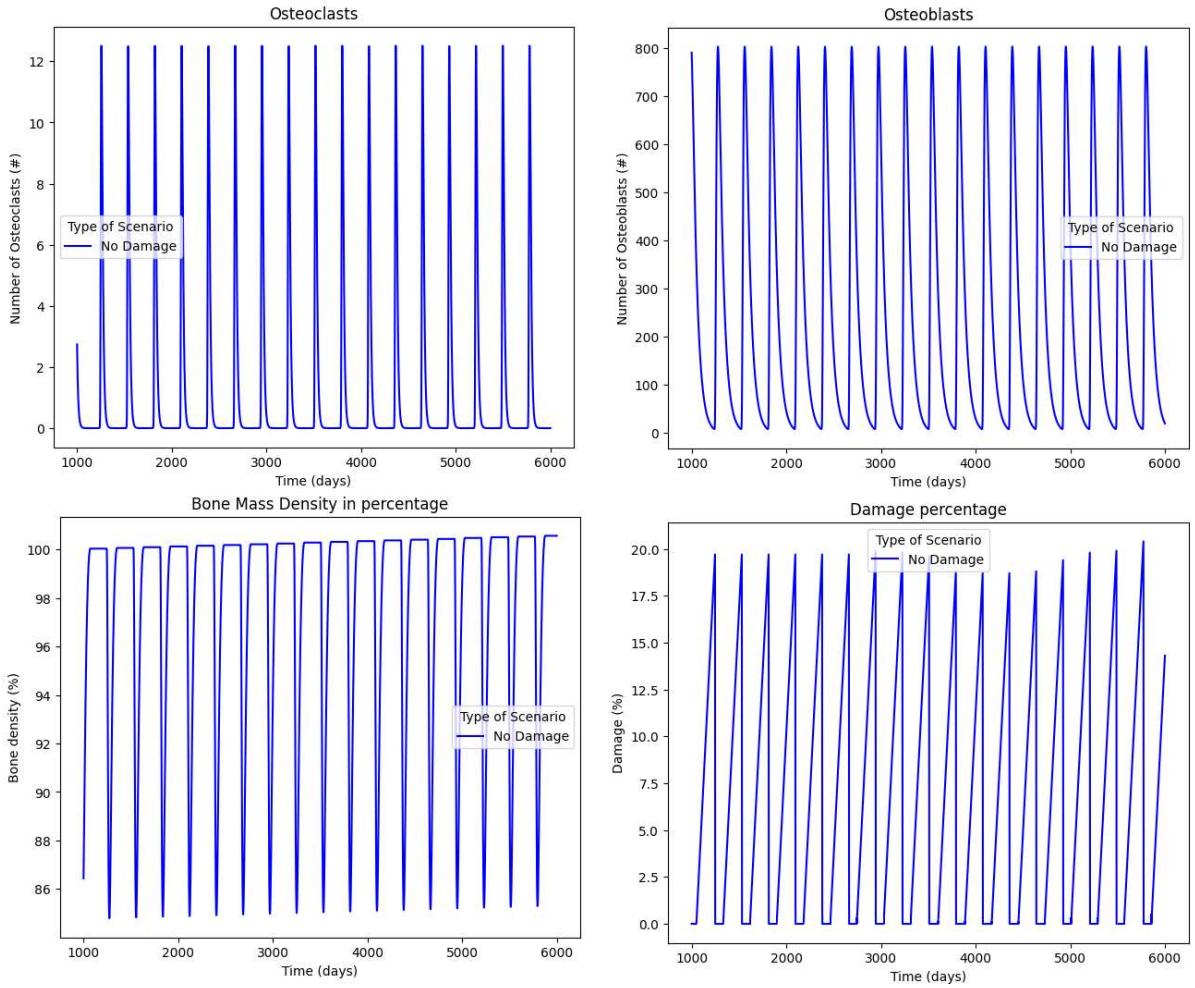

Figure 9: Tracking the bone remodeling cycle through the monitoring of a specific element, denoted as $e = 2215$, is illustrated in the figure. The graph comprehensively depicts osteoclasts, osteoblasts, bone density, and the percentage of damage over time.

.

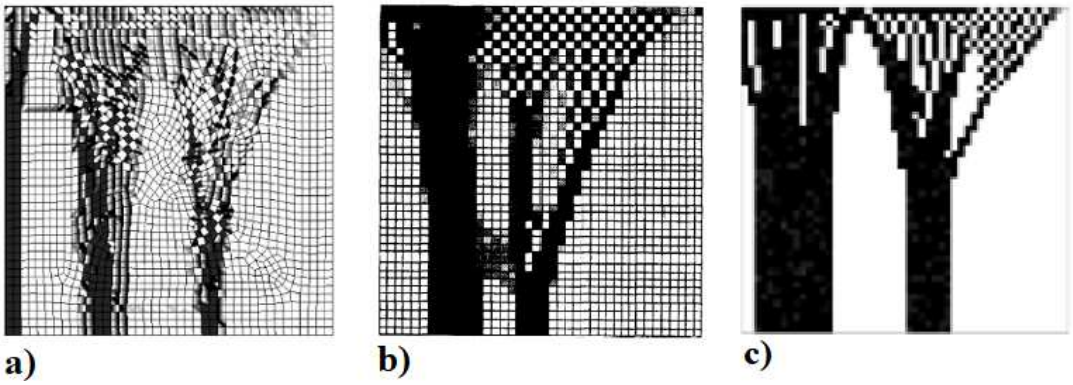

Figure 10: Comparison of bone remodeling results. (a) Structured mesh with continuous density distribution and trabecular-like branching from [10]; (b) Structured mesh showing checkerboard pattern due to element-based density update from [54]; (c) The result here obtained.

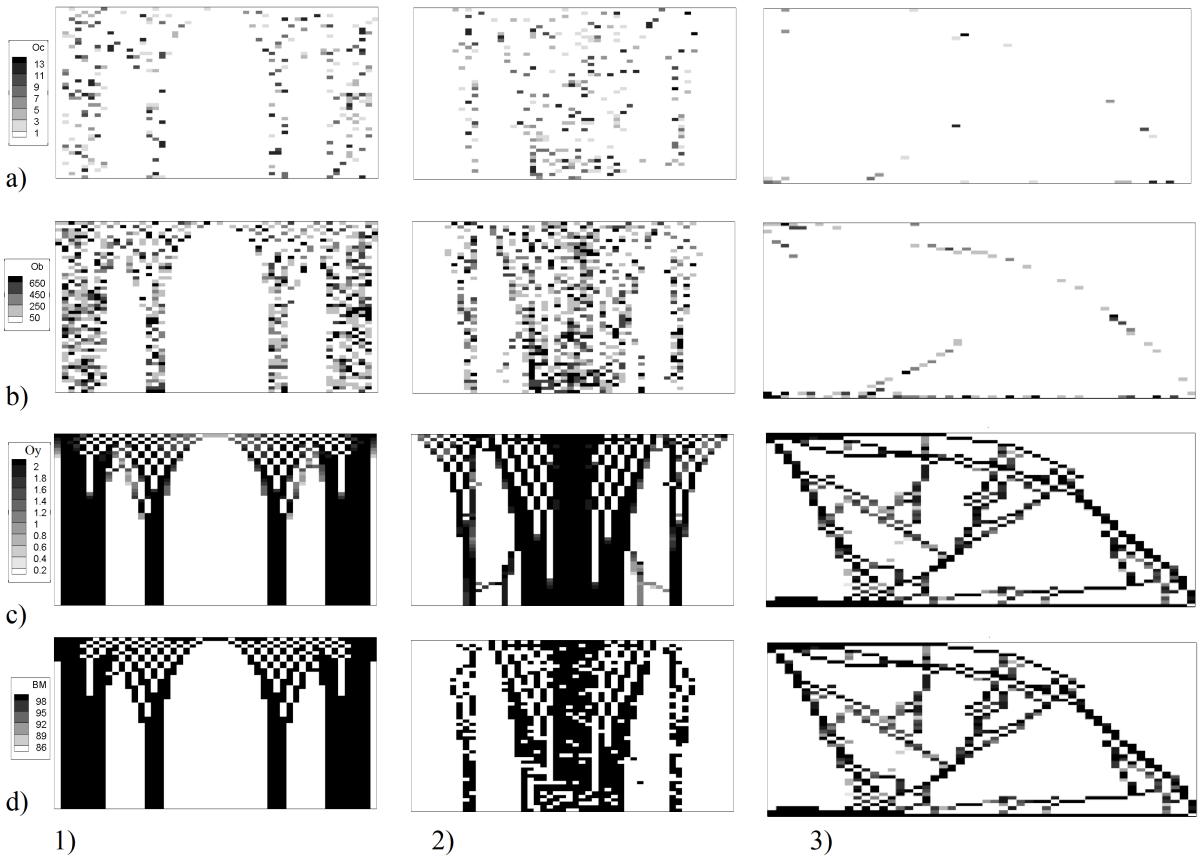

Figure 11: Spatial distribution of cellular activity and bone mass for three mechanical loading cases. Each column corresponds to a different example: (1) distributed load with maximum at both ends, (2) distributed load with central maximum, and (3) cantilever beam with a point load at the free end. Each row represents a biological component involved in bone remodeling: (a) osteoclasts—cells responsible for bone resorption, (b) osteoblasts—bone-forming cells, (c) osteocytes—mechanosensory cells embedded in the matrix, and (d) normalized bone mass, expressed as a percentage of the maximum density (100%). The figure illustrates how mechanical stimuli drive localized cellular responses and spatially guide the formation, maintenance, and removal of bone tissue, resulting in structures optimized for load-bearing performance.